Lateral loads carrying capacity and minimum thickness of circular and pointed masonry arches

N. Cavalagli, V. Gusella, L. Severini*

Department of Civil and Environmental Engineering, University of Perugia, Italy

Abstract

This paper aims to evaluate the limit equilibrium condition and the minimum thickness of masonry arches in presence of horizontal loads. The analysis fits into the frame of limit analysis referring to Heyman's theory. Two types of arches are analysed, the circular and pointed one. The loading system consists of vertical and horizontal loads, which refer respectively to the self-weight of the voussoirs and to the seismic actions. The collapse mechanism and the corresponding horizontal load multiplier are determined, in the condition of rigid abutments, as functions of the geometrical features of the structure. The results are supported by some simple experimental tests and a sensitivity analysis, which considers the effect of geometrical irregularity on the load multiplier.

Keywords: Masonry arch, Minimum thickness, Limit analysis, Collapse mechanism, Seismic action.

1. Introduction

The construction of arches and vaults has widely involved the architecture and engineering practice from the ancient centuries. There are direct evidences of using vaulted structures since several centuries before Christ, as in the Mesopotomian, Egyptian and Greek architecture, until coming to the Romans, which consolidated the construction practice of them by a huge

*Corresponding author

Email addresses: nicola.cavalagli@unipg.it (N. Cavalagli), vittorio.gusella@unipg.it (V. Gusella), lauraseverini@strutture.unipg.it (L. Severini)

The published version of the paper "N. Cavalagli, V. Gusella, L. Severini, Lateral loads carrying capacity and minimum thickness of circular and pointed masonry arches, International Journal of Mechanical Sciences, Volumes 115–116, 2016, Pages 645-656, ISSN 0020-7403" is available at: https://doi.org/10.1016/j.ijmecsci.2016.07.015.

using of the arch in structures and infrastructures. Nevertheless, the stability problem of an arch has always reserved some open questions about its nature, so that it has been widely studied throughout the centuries, and also during the last years, especially to improve the understanding of historical constructions, for their conservation and restoration.

It's well known that the first intuitions regarding the stability of an arch are related to Robert Hooke in 1676 [1], who claimed to have found "the true Mathematical and Mechanical form of all manner of Arches for Building" gaving the following solution "Ut pendet continuum flexile, sic stabit contiguum rigidum inversum–As hangs a flexible cable, so but inverted will stand the rigid arch" in an anagram form. This statement was the first of a series of studies concerning the catenary as the best shape for an arch; among them the works of Gregory [2], Bernoulli [3] and Stirling [4] must be mentioned. One of the most famous applications of this concept is referred to the study of Poleni for the stability of S.Peter's dome in Rome [5]. Effectively, in the same period also the research of a dome best shape was the object of several in-depth studies, especially for the analysis of the structural response [6, 7].

The 18th and 19th centuries were characterized by several contributions on the study of the stability and the minimum thickness of a masonry arch - Couplet [8] and Milankovitch [9] must be cited among others - which still today continue to be object of in-depth analyses [10, 11], with special attention also to the effect of stereotomy [12].

A turning point in studies on the stability of masonry buildings occurred in the early sixties of 20th century, when Jacques Heyman extended the limit analysis, initially developed for steel structures, to the so-called *Stone Skeleton*. The application of the classical approach of limit analysis to the masonry arch [13] requires the definition of *i)* equilibrium condition, *ii)* resistance criterion, *iii)* mechanism condition. The first *i)* and the second *ii)* correspond respectively to the individuation of a thrust line in equilibrium with external loads and anywhere contained in the boundary of the arch. The third condition *iii)* corresponds to a rotational mechanism, with hinges that grow at the edge of the thickness, and requires the assumption of the following hypothesis about the masonry [14]: masonry has no tensile strength, the compressive strength of masonry is infinite, sliding failure does not occur.

The stability of masonry arches is considered as a geometric problem, namely a right shape design is needed to achieve a safe state. Heyman [14] gives the law of the minimum thickness for the circular arch subjected just to self-weight, as a function of the angle of embrace. Heyman's solution is based on a static analysis, by writing equilibrium equations and tangency conditions with the assumption of considering the self-weight of the arch as uniformly distributed along its geometrical centreline. On the other hand, Milankovitch imposed the equilibrium equations by taking into account the right position of the centre of mass of the voussoirs. An interesting investigation on the comparison of such different hypotheses is shown in [15].

The analysis on the minimum thickness in presence of the self-weight has been recently extended also to pointed arches [16] and elliptical arches [17].

If on one hand the literature regarding the analysis of circular arches subjected to the self-weight is substantial, not much interest has been devoted to the structural response to the seismic actions. Among the first papers dealing with the masonry arch under seismic actions, it is worth mentioning the work of Franciosi [18], who developed a procedure based on limit equilibrium analysis in large displacements that considers horizontal equivalent static forces. However, it was necessary to wait the seminal paper of Oppenheim [19] for the definition of the dynamic equations of motion under inertial loads. In this work Oppenheim considered not only the occurring of the four-hinges mechanism, but also the subsequent non-linear dynamic response of the arch. This way was then followed by Clemente [20], who investigated the free vibrations and the response to harmonic base acceleration. The study of the dynamic behaviour has been later developed by considering the impact problem between the blocks [21] and by means of experimental tests [22]. More recently, the stability of masonry arches, characterized by different shapes and subjected to both vertical gravity and horizontal ground acceleration, has been investigated in [23, 24]. The collapse analysis of existing masonry arches is needed in order to assess their safety under the acting loads or environmental actions. If the structure is not able to stand the assigned loads or the safety margin is not guaranteed, strenghtening interventions are needed in order to increase its bearing capacity [25, 26, 27, 28], until the requirements of modern codes are satisfied.

In this work a numerical procedure for the prediction of the collapse condition of a structure made by rigid blocks has been performed, based on the limit analysis. The procedure has been applied to circular and pointed arches in order to investigate their capacity to withstand lateral loading.

Moreover, some experimental tests are performed to validate the procedure and a sensitivity analysis of the horizontal load multiplier is proposed, by varying the geometrical features of the circular and pointed arches.

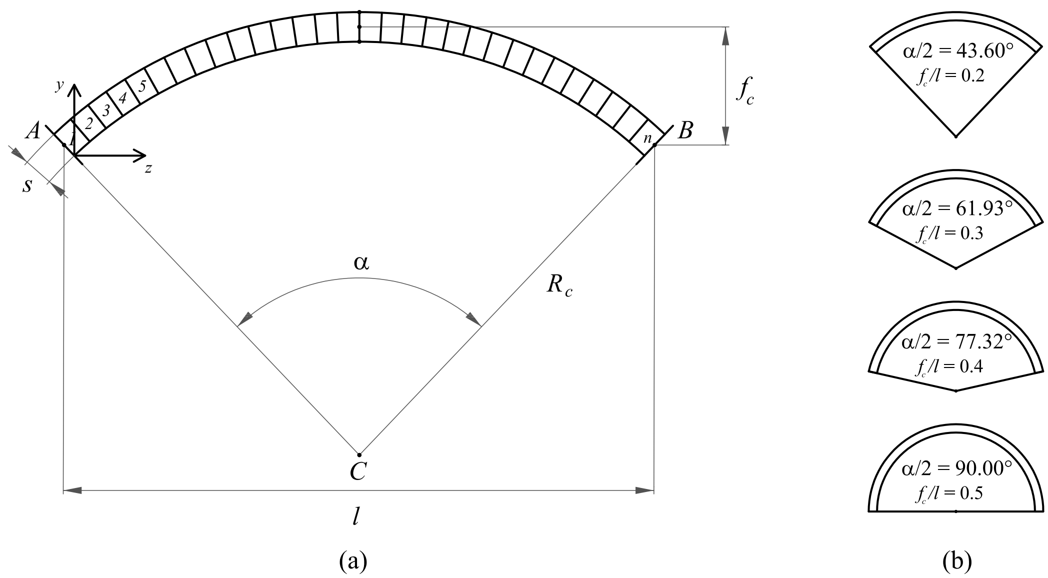

Figure 1: Geometry of the circular masonry arch (a) and analysed cases (b).

2. Circular arch

2.1. Geometrical description and numerical procedure

Let us consider the arch behaviour in its plane. The centreline of a circular arch is described by assigning the radius R_c and the central angle α or, alternatively, the span l and the rise f_c. Then the thickness s and the out of plane depth d uniquely identify the arch, as shown in Figure 1(a). In this paper four types of circular arch are analysed, three segmental and one semicircular, corresponding to the following f_c/l ratios: 0.2, 0.3, 0.4, 0.5 (Fig. 1(b)).

In the analysis, each arch is divided into n voussoirs, which are numbered from left to right. The resulting $n+1$ joints are obtained by radial cuts. In the following the generic voussoir will be identified by the index i and the generic joint by the index j. The geometrical description of the structure, referring to a system of Cartesian axes (z, y), requires the localization of the following points: the centroid G of each voussoir, the intrados I and extrados S points and the centroid P of each joint. Following the theory of Milankovitch [10], the centroid of the ith voussoir is calculated taking into account its effective geometry.

The loading system consists of vertical and horizontal forces, which represent respectively the self-weight F and the corresponding seismic action F_S. According to the hypotheses made in literature within this framework [18, 19, 20, 21, 22, 23], being the arch modeled as a rigid body, it is conceivable to consider that, in presence of an horizontal ground motion, it is subjected to the same level of acceleration. Then, by using limit analysis, it can be asserted that, also at collapse, the lateral inertial load for each voussoir is proportional to the vertical distribution of the mass by means of the same load multiplier k. Indeed the forces applied to the ith voussoir are:

$$F_i = \gamma_m \, A_i \, d \tag{1}$$

$$F_{S_i} = k \, F_i \tag{2}$$

where γ_m represents the masonry's specific weight and A_i the area of the ith voussoir in the arch plane. Without loss of generality it is assumed that the seismic action, i.e. the force F_{S_i}, is directed from left to right.

The presence of horizontal forces causes the development of four-hinges mechanisms at the collapse [19]. According to the safe theorem [14], the equilibrium of an arch is assessed if it is possible to reach a thrust line in equilibrium with the external loads which lies inside the boundaries of the arch, namely between the intrados and the extrados lines. By referring to limit analysis, it is possible to study the equilibrium condition of the arch at failure.

Let us assume a trial configuration of the position of the hinges M, Q, T, U corresponding to the m, q, t, u joints (Fig. 2). The analysis of the equilibrium condition is performed by means of a system of balance equations. Being V_U, H_U the vertical and horizontal internal forces at the hinge U, the equilibrium of moments around the remaining hinges gives:

$$\begin{cases} H_U(y_T - y_U) + V_U(z_T - z_U) - \sum_{i=1}^{n_{TU}} F_i(z_T - z_{G_i}) - k \sum_{i=1}^{n_{TU}} F_i(y_T - y_{G_i}) = 0 \\ H_U(y_Q - y_U) + V_U(z_Q - z_U) - \sum_{i=1}^{n_{QU}} F_i(z_Q - z_{G_i}) - k \sum_{i=1}^{n_{QU}} F_i(y_Q - y_{G_i}) = 0 \\ H_U(y_M - y_U) + V_U(z_M - z_U) - \sum_{i=1}^{n_{MU}} F_i(z_M - z_{G_i}) - k \sum_{i=1}^{n_{MU}} F_i(y_M - y_{G_i}) = 0 \end{cases} \tag{3}$$

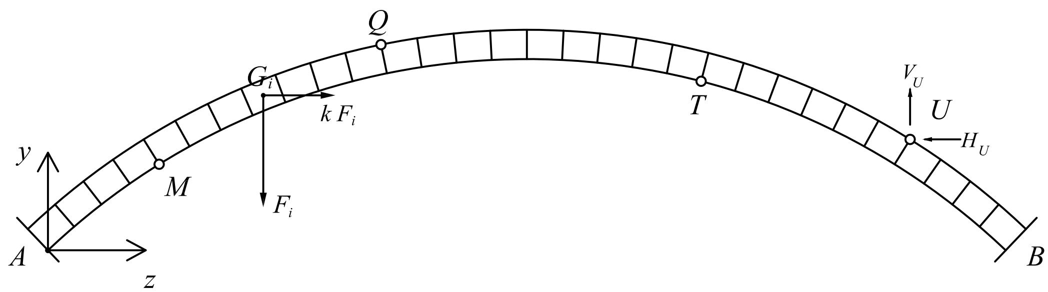

Figure 2: Generic four-hinge position associated to the collapse mechanism in presence of vertical and horizontal loads.

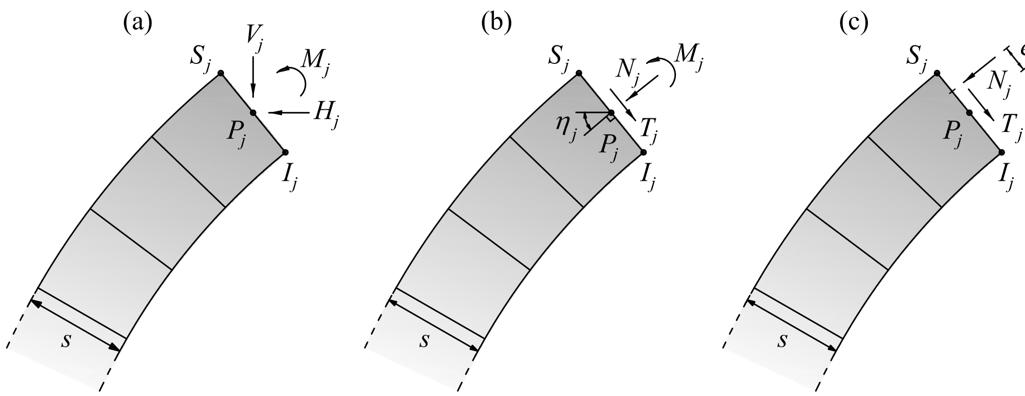

Figure 3: Stress state of the jth joint. Internal forces in the global reference system (a), in the joint reference system (b) and considering the eccentricity of the normal force (c).

where n_{TU}, n_{QU}, n_{MU} refer respectively to the number of voussoirs between the joints t, q, m and u. The Equation 3 is a determined system of three equations in the three unknowns V_U, H_U and the load multiplier k.

The system of forces must satisfy the strength criteria of the material, i.e. it is necessary to check that the trial set of hinges corresponds to a statically admissible configuration. The position of the thrust line is obtained joint-by-joint by the definition of the centre of pressure, namely of the eccentricity e_j of the normal force. By taking into account the position of the jth joint, the internal forces (Fig. 3(a)) are obtained by:

$$
\begin{cases}
H_j = H_U \mp k \displaystyle\sum_{i=1}^{n_{jU}} F_i \\
V_j = -V_U \pm \displaystyle\sum_{i=1}^{n_{jU}} F_i \\
M_j = V_U(z_U - z_{P_j}) + H_U(y_U - y_{P_j}) \mp \displaystyle\sum_{i=1}^{n_{jU}} F_i(z_{G_i} - z_{P_j}) + \\
\qquad\qquad\qquad\qquad\qquad\qquad \mp k \displaystyle\sum_{i=1}^{n_{jU}} F_i(y_{G_i} - y_{P_j})
\end{cases}
\tag{4}
$$

In the Equation (4), if the jth joint is at the left side of hinge U, the upper sign must be used, otherwise the lower one. By using the upper and lower sign for the cases $z_{P_j} < z_{I_j}$ and $z_{P_j} \geq z_{I_j}$ respectively (Fig. 3(b)), the normal force is known at each joint:

$$N_j = H_j \cos \eta_j \pm V_j \sin \eta_j \tag{5}$$

where η_j is the angle between the line perpendicular to the jth joint and the horizontal one. Finally, the eccentricity e_j of the normal force is given by (Fig. 3(c)):

$$e_j = \frac{M_j}{N_j} \tag{6}$$

In order to check if the line of thrust, obtained by linking the centres of pressure, is anywhere inside the masonry, the following condition must be verified at each joint:

$$-\frac{s}{2} \leq e_j \leq \frac{s}{2} \tag{7}$$

It should be noticed that the sign of equality holds only in correspondence of the hinges M, Q, T and U. As mentioned above, if (7) is satisfied, then the position of the hinges identifies the failure mechanism corresponding to the load multiplier. Otherwise, necessarily the configuration of the hinges must be changed and the equilibrium imposed again. The best practical choice is to find the joint p corresponding to the maximum eccentricity, i.e. where the distance between the centre line of the arch and the thrust line is maximum,

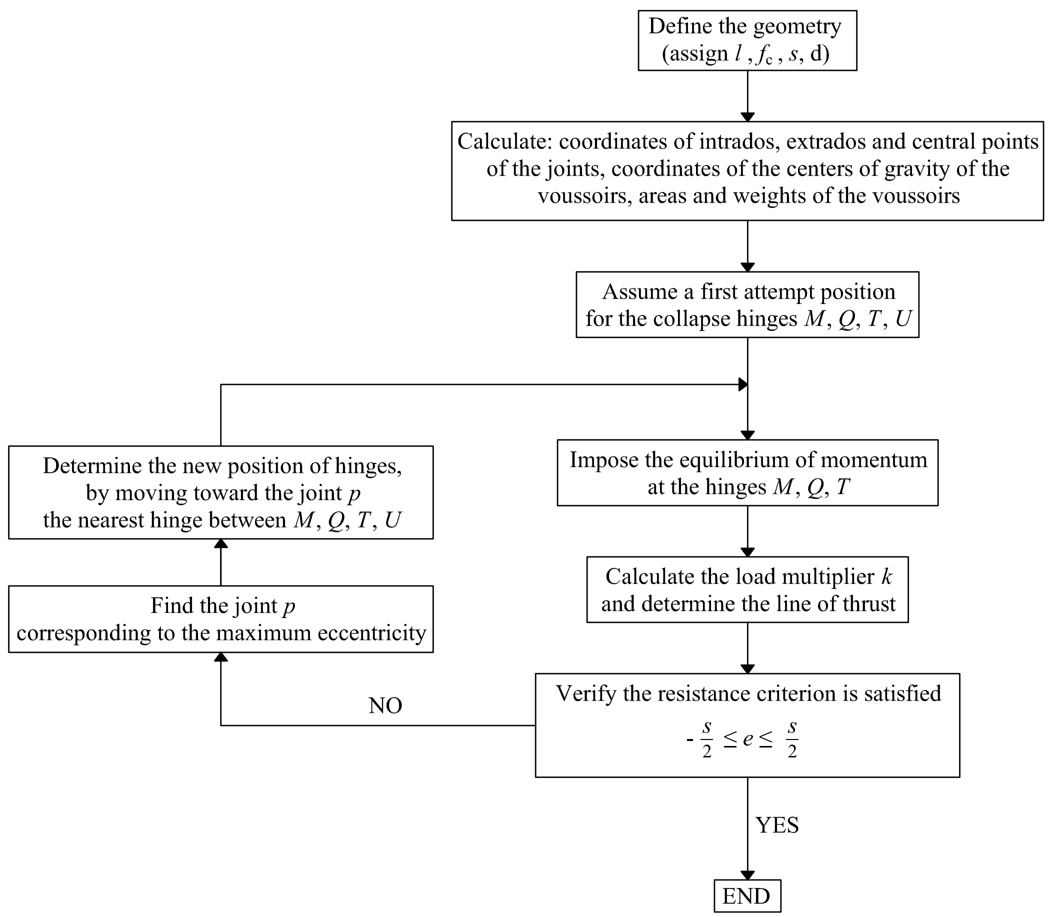

Figure 4: Scheme of the numerical procedure used in the analysis.

and to move the nearest hinge toward p [18]. With a few steps the right configuration is reached.

The proposed iterative procedure is summarized in the schematic block diagram of Figure 4. For more details see [29].

2.2. Limit analysis and minimum thickness

In order to illustrate the proposed procedure, the results relative to the four shapes of circular arches represented in Figure 1(b), characterized by the following values of the ratio f_c/l: 0.2, 0.3, 0.4 e 0.5, are reported in this paper. Considering that the proposed method is based on the discretization

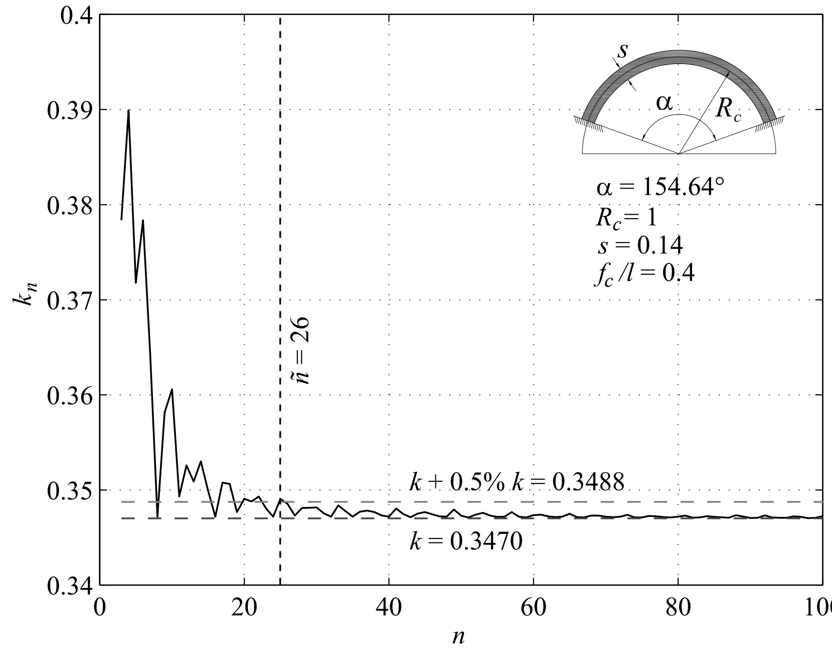

Figure 5: Load multiplier k_n of a circular arch depending on the number of voussoirs used in the discretization.

of the structure, the influence of the voussoir dimension on the value of the related horizontal load multiplier k_n has been analysed. A sensitivity analysis has been carried out for several geometries of arch, by varying the number of voussoirs n. The results of the case $f_c/l = 0.4$ and $s/R_c = 0.14$ are reported in Figure 5. It can be observed a significant variability of k_n in the range of low number of voussoirs, while for $n > \tilde{n}$ the difference between the multiplier related to a discretized arch and that corresponding to a continuous structure tends to zero. The value of $\tilde{n}$ was found for both circular and pointed arches. Hence, in the following analyses, a value of $n \gg \tilde{n}$ has been adopted in order to obtain results very close to the solution of the continuous model.

For each arch shape of Figure 1(b), the influence of the thickness dimension on the collapse has been investigated. In order to point out the horizontal load-carrying capacity of circular masonry arches, the relationship between the load multiplier k, the angle of embrace α and the dimensionless thickness s/R_c is shown in Figure 6. Each curve was obtained by setting a constant

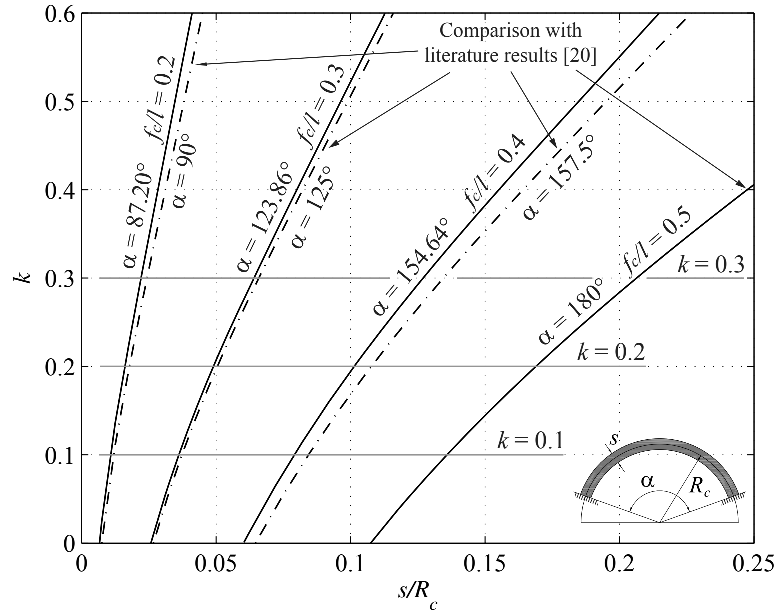

Figure 6: Load multiplier k of circular arches depending on the geometry.

value of the angle α, progressively increasing the parameter s/R_c and evaluating the corresponding value of the multiplier k at the collapse. The results obtained for the circular arches having $\alpha = 87.20°$ ($f_c/l = 0.2$), $\alpha = 123.86°$ ($f_c/l = 0.3$), $\alpha = 154.64°$ ($f_c/l = 0.4$) and $\alpha = 180°$ ($f_c/l = 0.5$) are represented by continuous lines. In order to validate the numerical procedure, also the curves obtained for the cases $\alpha = 90°$, $\alpha = 125°$ and $\alpha = 157.5°$ are represented, with dash-dot lines, revealing a good agreement with literature results [19, 20, 23]. Notice that for the same thickness, the multiplier k increases with the decreasing of the angle α. This means that, as was expected, the more the arch is lowered, the greater will be the resistance to horizontal actions, i.e. the earthquake.

In [14] Heyman studied the effects of geometrical properties on the stability of circular masonry arches subjected just to self-weight, providing the mathematical expression of the minimum thickness that the arch should have to stand, in terms of the angle of embrace and the dimensionless thickness. In this work the study has been extended to the case of presence of horizontal loads too, which are quantified through the load multiplier k.

By picking the points at constant values of k from Figure 6, it is possi-

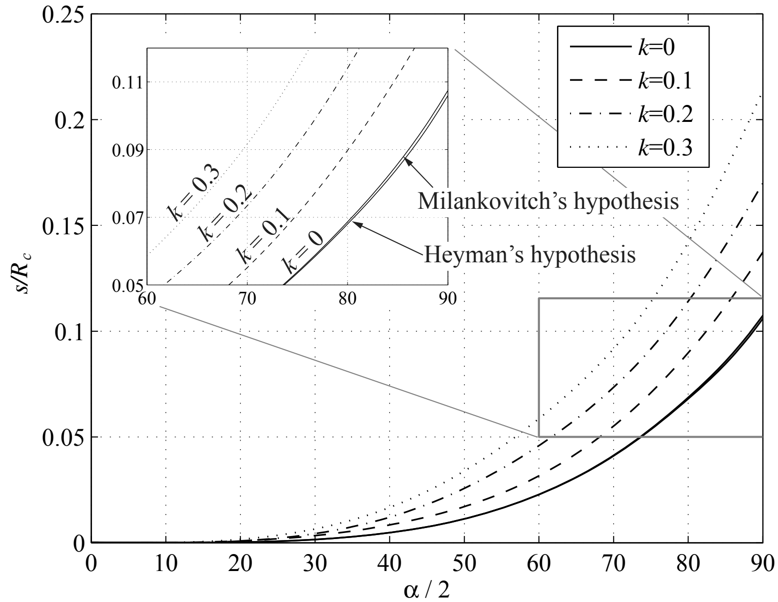

Figure 7: Minimum dimensionless thickness for circular arches subjected to vertical and horizontal loads.

ble to enter in the well-known minimum thickness diagram of Heyman [14] and obtain the curves which consider the effect of the horizontal load. Figure 7 depicts graphically the minimum thickness for the circular masonry arch in presence of an assigned horizontal load multiplier. The relationship is expressed between the half angle of embrace $\alpha/2$ and the dimensionless thickness s/R_c.

The continuous lines represent the literature results for the case of absence of horizontal loads and are obtained by means of both the theories of Heyman and Milankovitch. The discontinuous lines are obtained by considering the effect of horizontal loads at different values of k. It can be observed that greater values of thickness are necessary to withstand to greater values of horizontal loads and, by considering the individual curve, the minimum thickness increases with the increasing of the angle of embrace.

The variability of the geometrical properties of the arches affects the kinematic mechanisms. In Figure 8 the thrust lines at the collapse for the analysed circular arches (Fig. 1(b)) are represented, by varying the thickness, as functions of the dimensionless curvilinear abscissa ξ. In the analyses, the

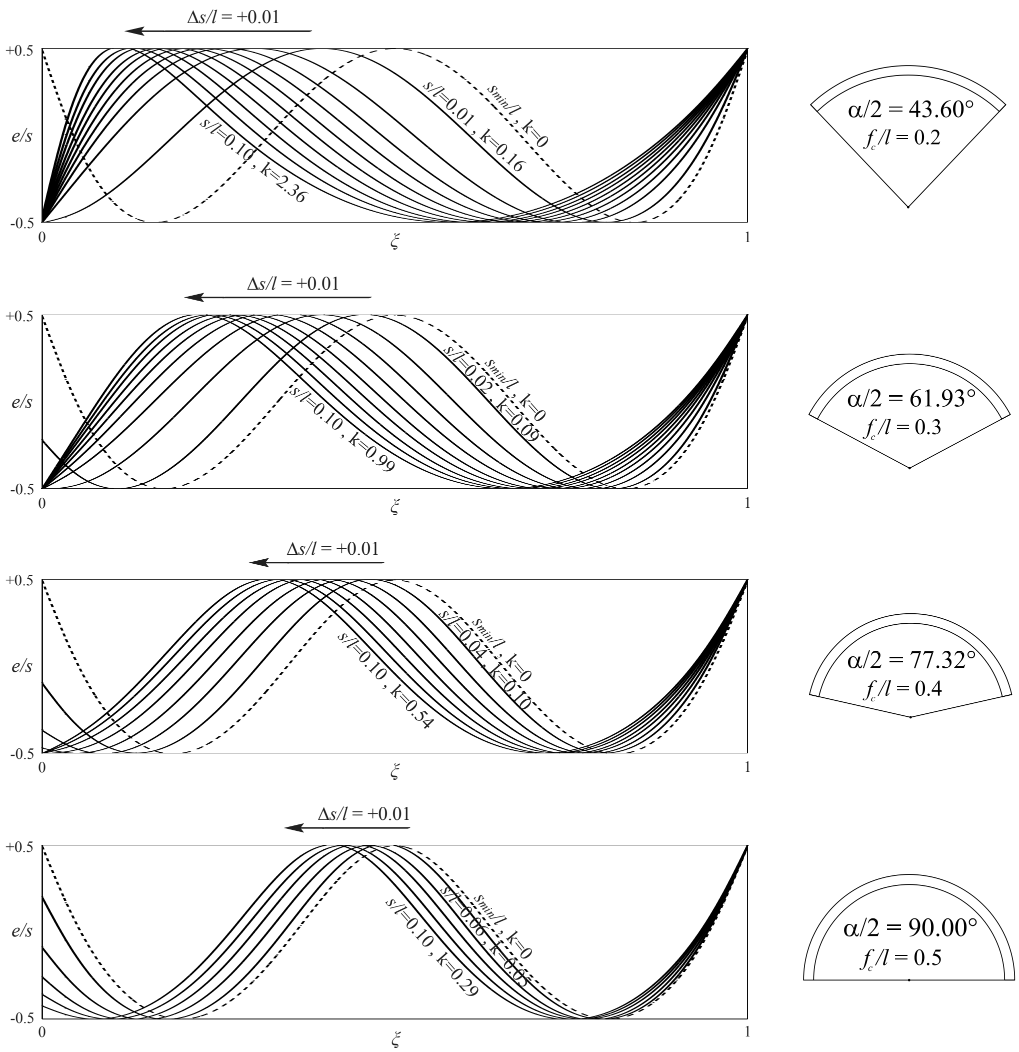

Figure 8: Thrust lines for circular arches with thickness variation.

thickness and its variation are normalized with respect to the span of the arch, instead to the radius of curvature, to simplify the future comparisons with the results obtained on pointed arches. The abscissa ξ is calculated by considering its origin in the centre of the left-springing joint of the arch, and the ordinate represents the dimensionless eccentricity e/s of the centre of pressure. The collapse mechanism can be quickly identified, because the hinges correspond to the tangent points of the curves to the horizontal lines of equation $e/s = \pm 0.5$, which represent the extrados and intrados lines respectively. The dashed line represents the thrust line of the arch subjected to the only self-wight. It could be noticed that a non-zero load multiplier k causes a loss of symmetry in the mechanism and then a reduction of the number of the hinges that lead to the collapse. In the case of $k = 0$ the well-known five-hinges mechanisms are reached: hinges grow at the extrados in correspondence of the keystone and springings, and at the intrados in correspondence of the haunches. In presence of horizontal loads four hinges are sufficient to activate a mechanism. The hinges of the condition $k = 0$ moves from right to left as the load multiplier increases, namely in the opposite direction with respect to the horizontal loads.

3. Pointed arch

3.1. Geometrical description

Unlike the circular arch, a pointed arch requires three parameters, other than the thickness s and the out of plane depth d, to be geometrically described. Actually, the structure is determined by assigning the radius R_p, the slope angle at the crown θ_{min}, which is strictly positive, and the slope angle at the skewback θ_{max}, with $\theta_{max} \leq 90°$ (Fig. 9). If $\theta_{max} < 90°$ the arch is named segmental pointed arch. The position of the centre C of the geometrical construction defines the eccentricity e_p as the difference between the radii R_p of the pointed arch and R_c of the subtended circular arch. In this way, as known in literature, three types of pointed arches can be identified: drop arch (or obtuse arch) with $0 < e_p/R_c < 1$ ($1 < R_p/R_c < 2$), equilateral arch with $e_p/R_c = 1$ ($R_p/R_c = 2$) and lancet arch with $e_p/R_c > 1$ ($R_p/R_c > 2$). On the other hand, a pointed arch could be defined by the span l, the rise f_p and the slope angle at the skewback θ_{max}. The relations between the span, the rise and the previous geometrical features are the following

$$l = 2R_p(\sin\theta_{max} - \sin\theta_{min}) \tag{8}$$

$$f_p = R_p(\cos\theta_{min} - \cos\theta_{max}) \tag{9}$$

3.2. Collapse modes of pointed arch

The kinematic mechanisms in presence of the only self-weight are symmetrical and characterized by five or six hinges. The presence of the hinge at the crown is obviously characteristic of the five-hinges mechanism and depends

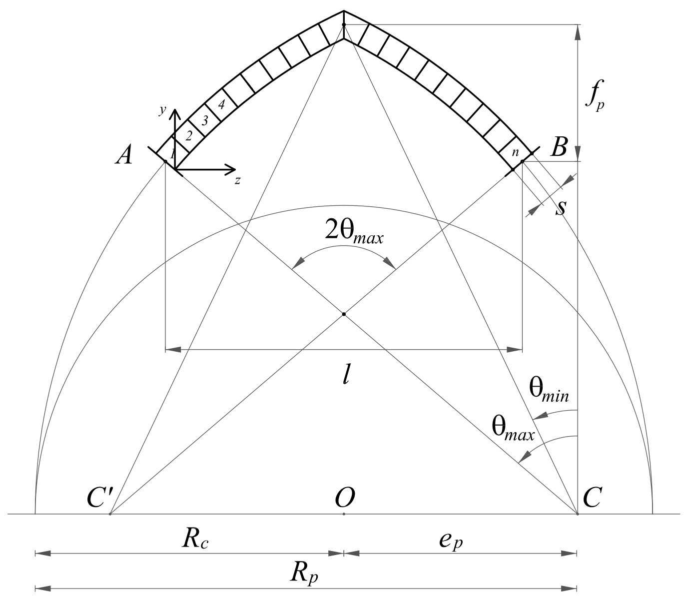

Figure 9: Geometry of the pointed masonry arch.

on the slenderness of the arch. When the lateral loads begin to act, e.g. from left to right, four-hinges mechanisms occur, so as to create a kinematic chain. Being M, Q, T and U the sequence of hinges from left to right, in spite of the case of circular arch, the extreme right hinge U will not always take place at the right springing B, as the extreme left hinge M which may occur within the arch. In this way, the performed numerical analysis has shown that four types of collapse modes can be identified: no-springing, left-springing, right-springing and two-springing (Fig. 10). The "no-springing" mode has all the hinges placed inside the arch (namely there aren't any hinges at the springings) and is typical for slender arches having low ratios of s/R_p (Fig. 10(a)). In the case of a segmental pointed arch, it is possible that the first hinge M is directly placed at the left springing (Fig. 10(b)). This observation leads to understand that arches with the same R_p, θ_{min} and s but different values of θ_{max} can be characterized by the same collapse multiplier k which causes the same collapse mechanism (compare the arches of Fig. 10(a) and (b), which differ for the value of the angle θ_{max}). By increasing the thickness, the extreme right hinge U rapidly moves to the springing B and the collapse mode becomes of "right-springing" (Fig. 10(c)) if the first hinge M is inside the arch or, alternatively, of "two-springing"(Fig. 10(d)) if the hinge M was

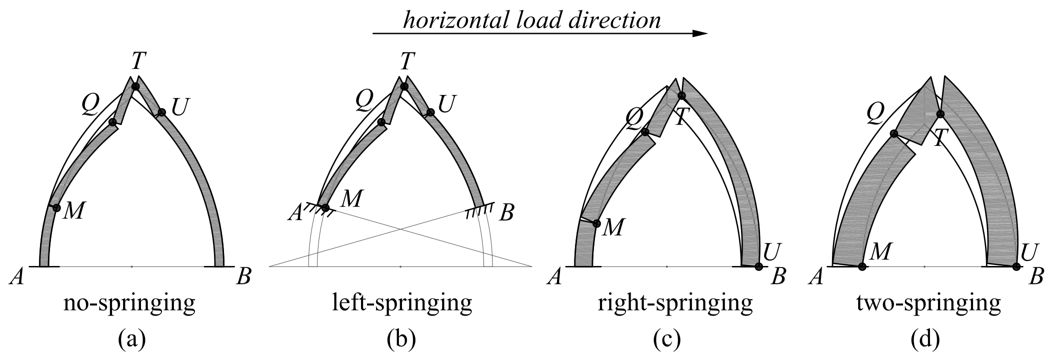

Figure 10: Schematic illustration of the collapse modes occurring in pointed arches subjected to lateral loads.

previously placed at the left springing. From the "right-springing" mode, with a further increase of thickness also the left hinge M slowly slides to the springing A and the "two-springing" mode occurs.

The sliding of the hinge U to the springing B, i.e. the passage from "no-springing" or "left-springing" mode to "right-springing" or "two-springing" mode, causes a significant loss of capacity to withstand the lateral loads. In other words, if the hinge U is at the right springing, a major increment of thickness is necessary, in comparison to the other cases, to withstand the same increment of lateral loads. The passage from "right-springing" to "two-springing" mode, or in some cases from "no-springing" to "left-springing" mode, doesn't cause significant effects as in the previous case.

3.3. Lateral loads multiplier and minimum thickness

In order to justify the collapse modes previously introduced and highlight their correlation with the lateral loads multiplier and the minimum thickness, the results related to two cases are reported: a drop arch with $e_p/R_c = 0.65$ ($R_p = 1.65\,R_c$) and a lancet arch with $e_p/R_c = 1.5$ ($R_p = 2.5\,R_c$). The procedure have been applied to arches with fixed angle of embrace $2\theta_{max}$ at different values of thickness. The slope angle at the skewback, starting from the value $\theta_{max} = 90°$, has been decreased at constant intervals up to its minimum possible value. In Figure 11 the curves of the minimum horizontal loads multiplier for the case with eccentricity $e_p/R_c = 0.65$ are represented.

From the results of Figure 11 it is possible to extract the curves of minimum thickness at different levels of horizontal loads multiplier as shown in Figure 12. It can be observed that the minimum dimensionless thickness converge to zero for $\theta_{max} \to \theta_{min}$. The curve with $k = 0$ is characterized by an horizontal branch in a range of the angle of embrace of about $62° \div 85°$, due to the type of collapse mode involved. The kinematic chain is symmetrical with five hinges for arches with big eccentricity and six hinges for arches with small or medium eccentricity. The arch in exam can be considered of medium eccentricity, presenting at $\theta_{max} = 90°$ a six-hinges mechanism. By decreasing θ_{max} also the minimum thickness diminishes, until a five-hinges mechanism occurs with the presence of an hinge at the crown. However, the lowest hinges are not at the skewbacks of the arch, so that θ_{max} can further decrease without affecting the collapse condition of the arch, until the two hinges are reached by the springing line. This phenomenon can be defined as a stationary collapse configuration, which is independent of the geometry of the arch in the specific range of θ_{max}. At lower values of θ_{max} correspond five-hinges mechanisms with hinges at the skewbacks and thickness increasingly smaller to zero. The phenomenon previously described doesn't appear in presence of horizontal forces (Fig. 12, $k > 0$), due to the asymmetry of the loads which determines asymmetric mechanisms and a continuous shifting of the hinges along the extrados and intrados lines to reach the equilibrium condition. The path of some curves of Figure 11 highlights the collapse mode which occurs depending on the slenderness, the angle of embrace and the level of horizontal loads. Within this context, the plane of the graph has been filled with two different levels of grey to identify the presence of the hinge U at the right springing (low level of grey) or not (high level of grey), since it has been noticed above that the position of hinge U greatly influences the horizontal load-carrying capacity. The collapse modes of Fig. 10(a) and (b) obviously correspond to the high level of grey, while those of Fig. 10(c) and (d) are of low level of grey. When the collapse mode under the only self-weight ($k = 0$) is of six-hinges, as in the case of $\theta_{max} = 90°$, if k starts to increase the kinematic chain become of four-hinges with the presence of an hinge at the right springing. This response is quite similar to circular arches, which are always characterized by the presence of an hinge at the right springing. This behaviour is typical for pointed arches with small and medium eccentricity. When the collapse mode under the only self-weight ($k = 0$) becomes of five-hinges, i.e. by considering values of the slope angle at the skewback $\theta_{max} < 90°$, if the load multiplier k is increased, the kinematic mechanism can be either of "no-springing" or "left-springing" (high level of grey). Then, by further increasing the lateral loads the kinematic mechanism become of "right-springing" or "two-springing" (low level of grey).

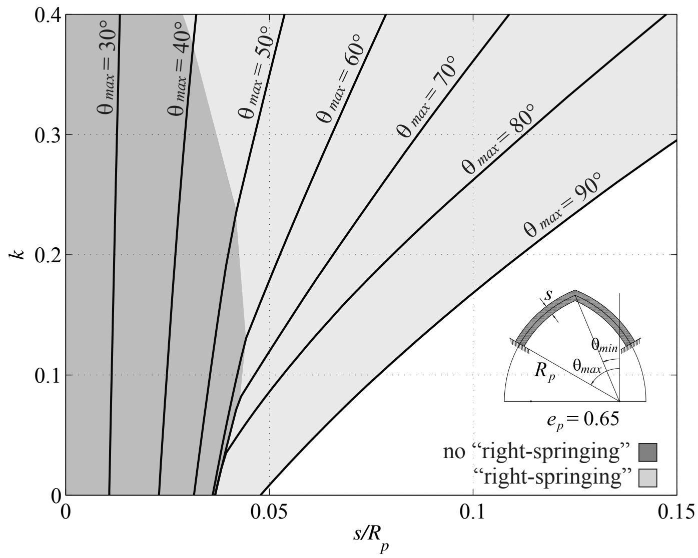

Figure 11: Minimum horizontal loads multiplier of pointed arches with eccentricity $e_p/R_c = 0.65$, angle of embrace $2\theta_{max}$ and slenderness s/R_p.

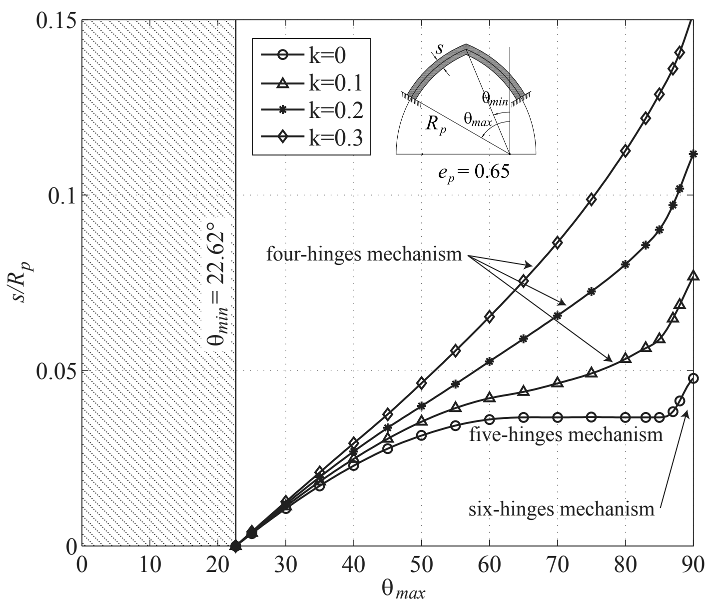

Figure 12: Minimum dimensionless thickness of pointed arches with eccentricity $e_p/R_c = 0.65$, angle of embrace $2\theta_{max}$ at different values of the horizontal loads multiplier k.

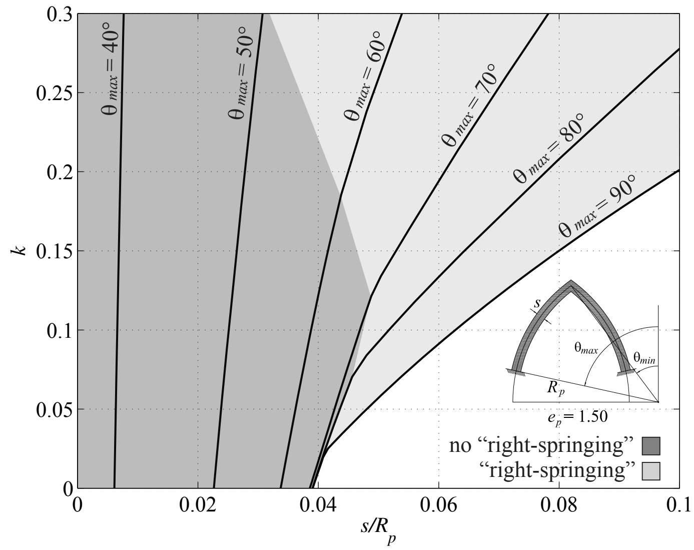

Figure 13: Minimum horizontal loads multiplier of pointed arches with eccentricity $e_p/R_c = 1.5$, angle of embrace $2\theta_{max}$ and slenderness s/R_p.

The results of the analysis carried out on the lancet arch are shown in Figures 13 and 14. In this case the collapse mode under the only self-weight is always of five-hinges as the angle of embrace changes. According to the previous observations, this is shown by the stationary branch of the curve at $k = 0$ in the range of about $75° \div 90°$ (Fig. 14). As the horizontal loads start to act the kinematic mechanism become of four-hinges with “no-springing” or “left-springing” mode for every segmental arch. By further increase the value of k the limit behaviour is similar to that described before (Fig. 13).

In Figure 15 the thrust lines of both the analysed arches with $\theta_{max} = 90°$ are shown, by varying the thickness values normalized to the span of the arch. The previous considerations about the kinematic mechanisms can now be observed in the tangent points with the extrados and intrados lines.

These results have highlighted the strong dependence of the lateral load carrying capacity of pointed arches from the geometrical parameters - as well as the eccentricity, the angle of embrace and the thickness - which determine the related collapse mechanism.

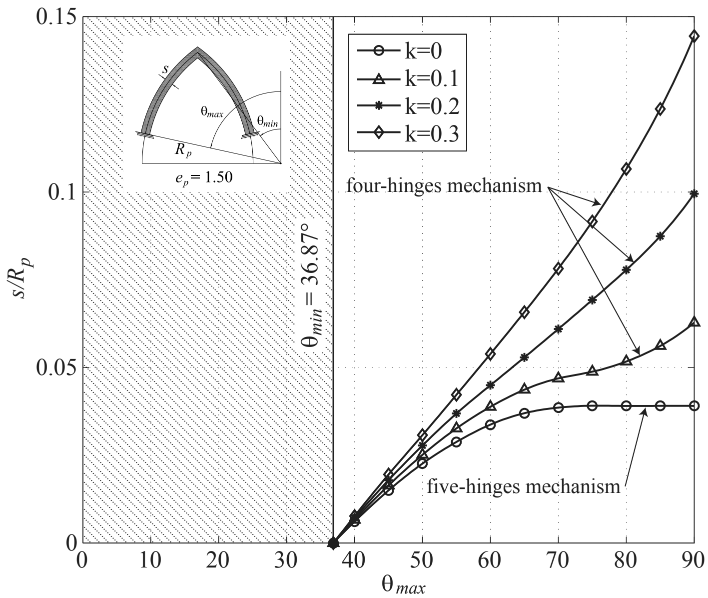

Figure 14: Minimum dimensionless thickness of pointed arches with eccentricity $e_p/R_c = 1.5$, angle of embrace $2\theta_{max}$ at different values of the horizontal loads multiplier k.

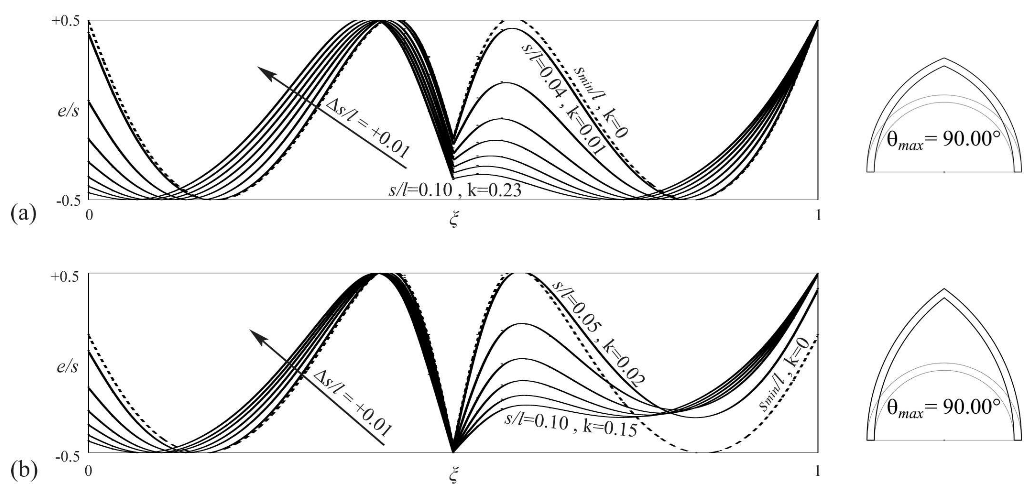

Figure 15: Thrust lines of pointed arches with $e_p/R_c = 0.65$ (a) and $e_p/R_c = 1.50$ (b), having $\theta_{max} = 90°$, with thickness variation.

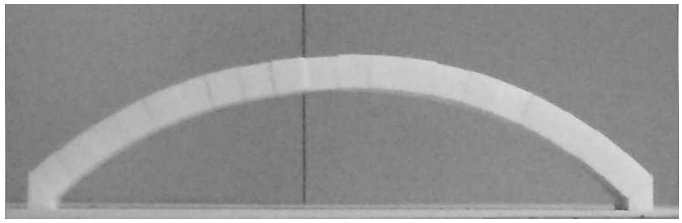

Figure 16: Image of the segmental circular arch with a ratio of $f_c/l = 0.2$ subjected to the experimental test.

4. Experimental tests

4.1. Circular arch

In order to validate the numerical procedure, simple experimental tests have been carried out on models of arch realized in XPS material (extruded polystyrene foam). A segmental circular arch has been tested, consisting of 20 voussoirs and having the following nominal sizes: span 50 cm, rise 10 cm ($f_c/l = 0.2$), thickness 3 cm ($s/l = 0.06$) and depth 5 cm (Figure 16). The lateral forces have been introduced by tilting the base plane, so that the load multiplier k could be obtained from the inclination angle φ of the plane itself.

In Figures 17(a) and (b) the numerical results are represented. Figure 17(c) shows the instant at the collapse of the segmental arch, in which the position of the hinges are pointed out so that the kinematic mechanism can be easily compared. The frame has been captured from a video-clip of the test. Numerical and experimental results are in quite good agreement in terms of the kinematic mechanism, but a reduction of the load multiplier is obtained. Similar experiments were carried out by other authors [19], who, in turn, observed a substantial reduction of the minimum horizontal acceleration which caused the collapse. Also Romano and Ochsendorf [16] recently asserted that the difference between the numerical and experimental results in this kind of tests could be not negligible. In fact, the numerical model is assumed to be characterized by rigid voussoirs with perfect edges and corners, while actual samples are affected by geometrical and material imperfections that influence the results. Moreover, the assembly of the specimen involves several constructive imperfections, so that the actual values of span and rise could differ from the nominal ones.

In order to investigate the influence of the geometrical uncertainties on the load multiplier, a sensitivity analysis has been performed by considering

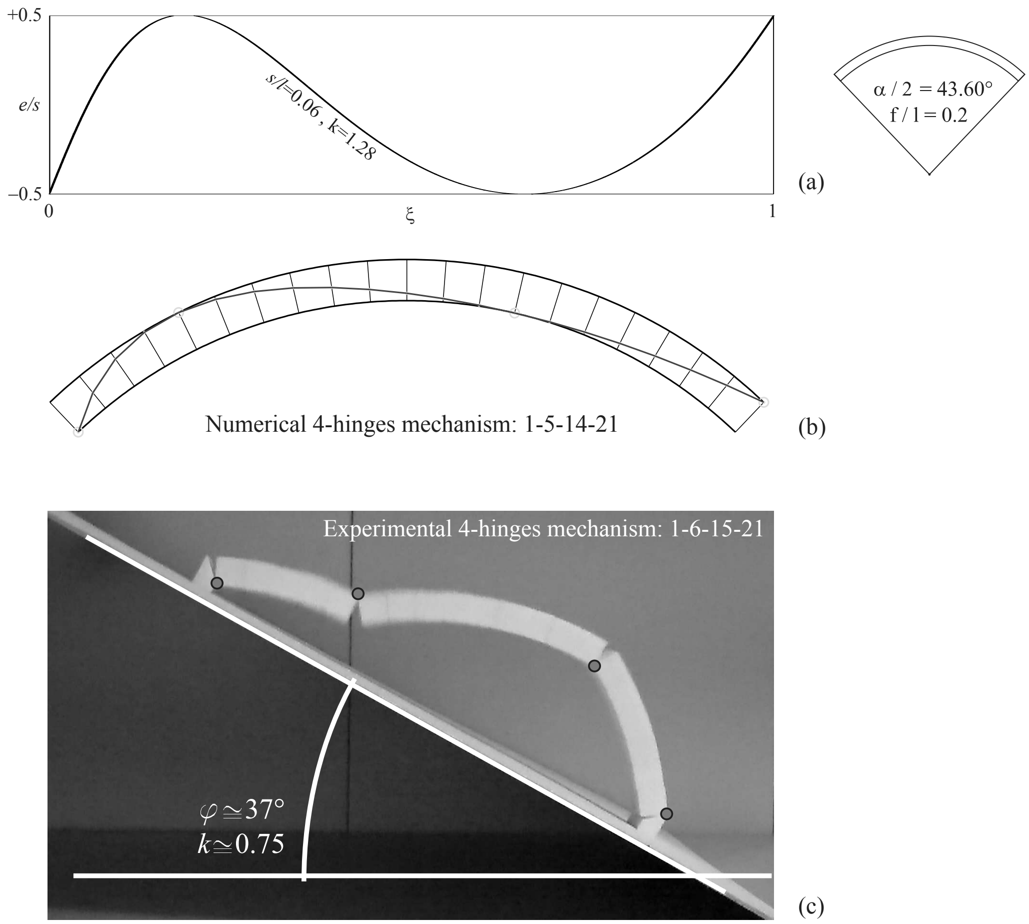

Figure 17: Kinematic mechanism of the segmental circular arch (nominal size: $f_c/l = 0.2$, $s/l = 0.06$) subjected to vertical and horizontal loads: numerical results (a)-(b) and experimental test (c).

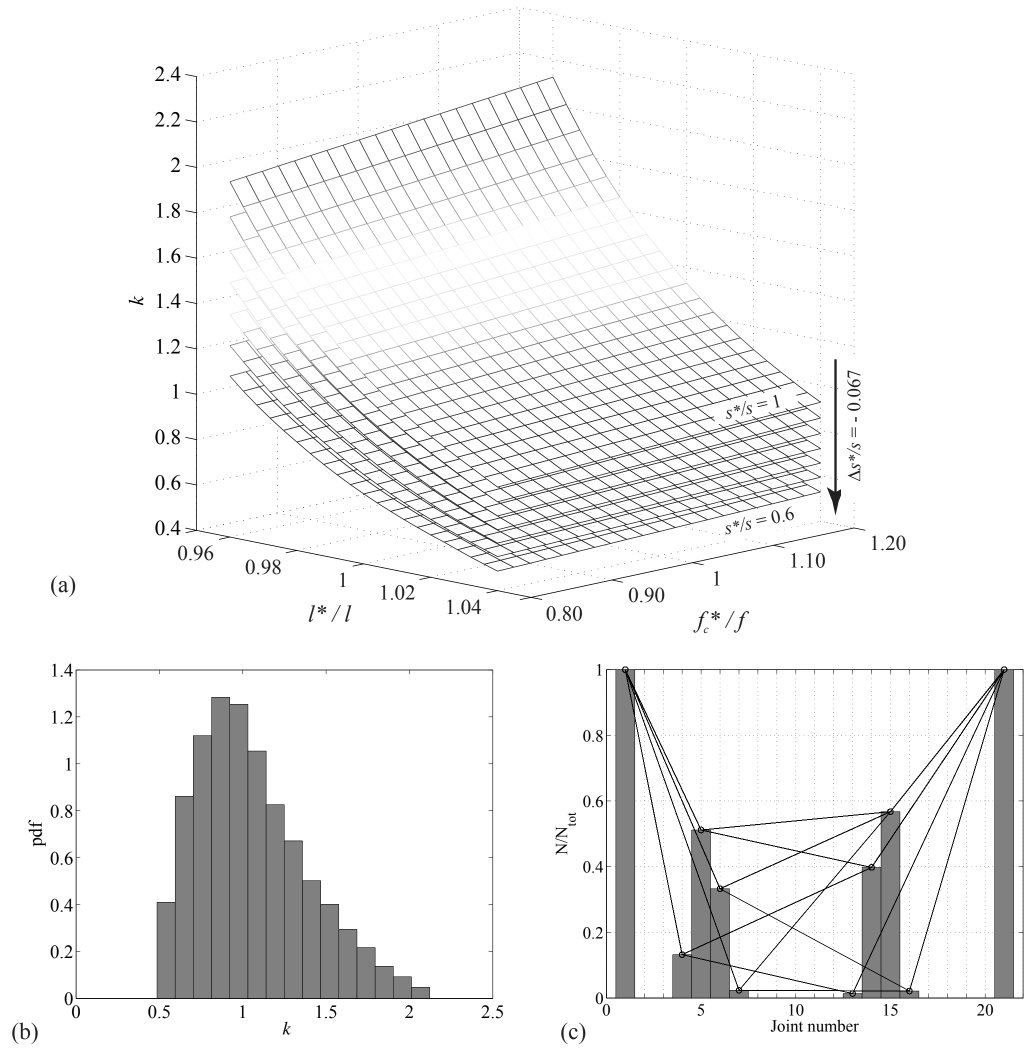

Figure 18: Segmental circular arch with nominal ratio $f_c/l = 0.2$. Results of the sensitivity analysis on the load multiplier by varying the geometrical parameters (a), estimation of the probability density function of the load multiplier (b) and representation of the kinematic mechanisms variability (c).

the variability of span, rise and thickness. In particular, uniform probability distributions around the nominal values have been adopted for the geometrical parameters l and f_c. Also for the thickness s a uniform probability distribution has been used, assuming upper bound of the range variability equal to its nominal value. In Figure 18 the results are shown as functions of the variables l^*, f_c^* and s^*, normalized with respect to the nominal corresponding values. The variability range magnitude of the ratios l^*/l and f_c^*/f_c is of 4% and 20% respectively, while the normalized thickness ratio s^*/s has been reduced with constant step of $\Delta s^*/s = 0.067$. The sensitivity analysis shows a low dependence of the load multiplier on the rise variability and a high dependence on the thickness and span (Figure 18(a)). Figures 18(b)-(c) show an estimation of the probability density function of the load multiplier and the type of kinematic mechanism which can occur respectively. From the analysis of the distribution shown in Figure 18(b), it can be observed that the experimental value of the load multiplier k is in the range $\mu \pm \sigma$, being the mean value $\mu = 1.056$ and the standard deviation $\sigma = 0.33$. By following the path of each broken line of Figure 18(c), the possible kinematic mechanisms can be observed. In fact, each line links four hinges located at the related joints, numbered in the abscissa axis from 1 to 21. The variable N represents the number of occurrences of the considered hinge in the jth joint, with $j = 1$ to 21, and N_{tot} is the total number of samples.

The numerical analysis highlights a strong sensitivity of the results in terms of the load multiplier, while the kinematic mechanisms are quite independent of geometrical properties, with the exception of the second and third hinge. In fact, the first and the fourth hinge are always at the springings of the arch, namely in the first and last joint respectively. The location of second and third hinges is limited to a small range of joints, with high frequencies in the $5th$ and $15th$ respectively. By the comparison between Figure 17 and Figure 18, it can be asserted that the experimental and numerical results are in good agreement, if the geometrical uncertainties are taken into account.

4.2. Pointed arch

An experimental test has been carried out on a model of pointed arch with $e_p/R_c = 1.5$ and $\theta_{max} = 90°$. The arch consists of 30 voussoirs and has the following nominal sizes: span 50 cm, rise 50 cm ($f_p/l = 1.0$) and thickness 5 cm ($s/l = 0.1$). The depth of the model is 5 cm (Figure 19).

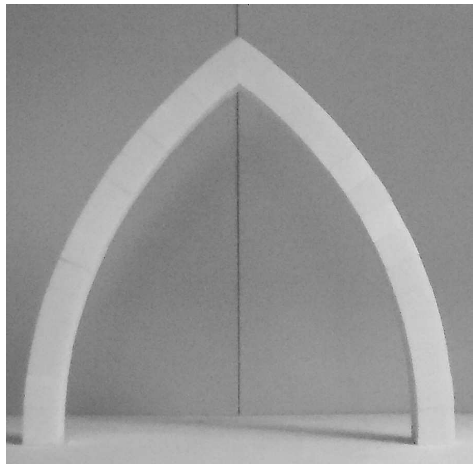

Figure 19: Image of the pointed arch subjected to the experimental test.

The comparison between experimental and numerical results is shown in Figure 20. In this case the load multiplier and the kinematic mechanism derived by the test are in a good agreement with the numerical results. The greater thickness of the model may have reduced the experimental uncertainties of the blocks and of the construction phase of the arch.

For the pointed arch, the sensitivity analysis has been carried out by considering a magnitude of the variability range for the ratios l^*/l and f_c^*/f_c of 4%, while the normalized thickness ratio s^*/s has been reduced with a constant step $\Delta s^*/s = 0.04$. The results highlights a very low dependence of the load multiplier on the span and rise variability and a high dependence on the thickness (Figure 21(a)). By referring to the distribution shown in Figure 18(b), also in this case the experimental value of the load multiplier k is in the range $\mu \pm \sigma$, being the mean value $\mu = 0.1$ and the standard deviation $\sigma = 0.02$. The kinematic mechanisms are well defined, excepting the position of the first hinge (Figure 21(c)).

By a close observation of the test, according to the authors, the main reason which causes the gap between experimental and numerical results is the unavoidable reduction of the nominal thickness, related to the manufacturing of the blocks and the construction of the arch model. In fact, little geometrical perturbations, also in just one of the joints, determine significant variations of the results.

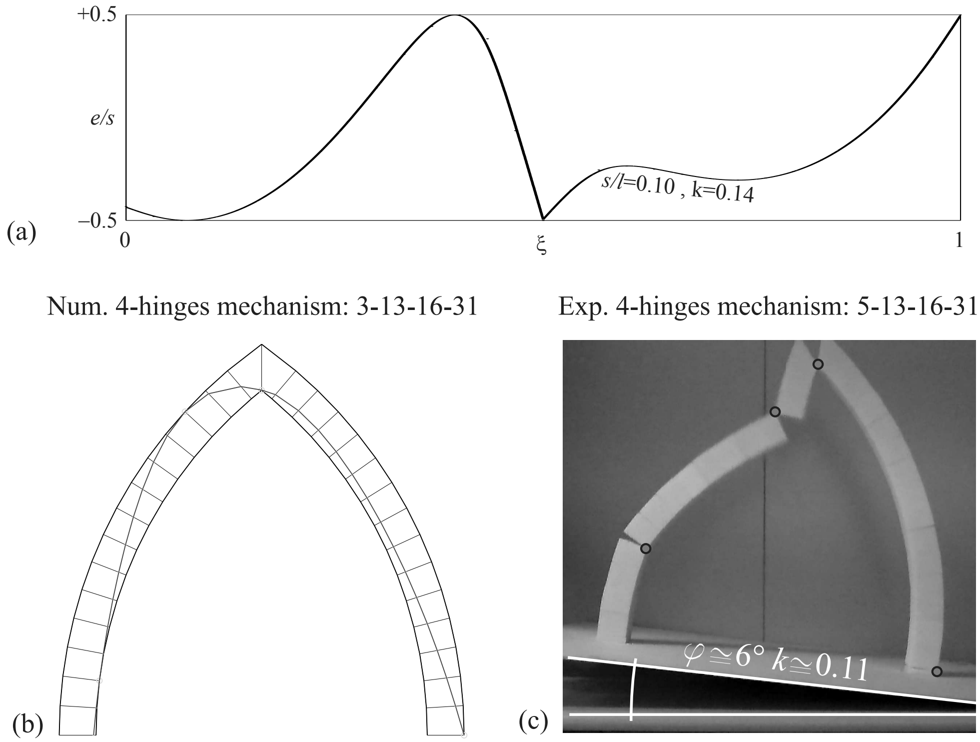

Figure 20: Kinematic mechanism of the pointed arch (nominal size: $f_p/l = 1.0$, $s/l = 0.1$) subjected to vertical and horizontal loads: numerical results (a)-(b) and experimental test (c).

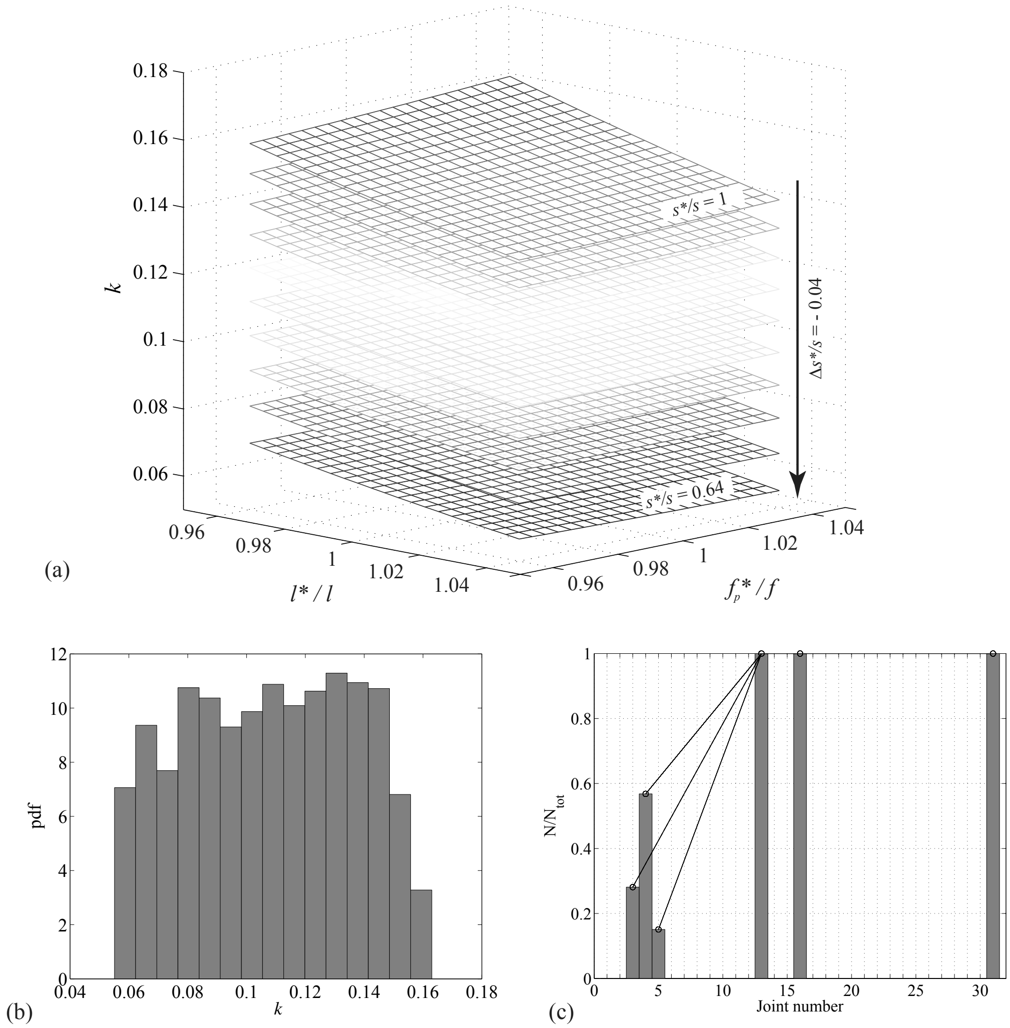

Figure 21: Pointed arch with nominal ratio $f_p/l = 1.0$. Results of the sensitivity analysis on the load multiplier by varying the geometrical parameters (a), estimation of the probability density function of the load multiplier (b) and representation of the kinematic mechanisms variability (c).

5. Conclusions

In this paper the collapse condition of circular and pointed masonry arches has been analysed in presence of vertical and horizontal loads.

The proposed procedure led to evaluate the collapse mechanism and multiplier depending on the geometrical properties of the arch. In particular, for the pointed arch some classes of mechanism have been identified and the transition between them evaluated as a function of the slenderness of the arch. The minimum thickness has been determined depending on the horizontal load multiplier and geometrical features. The obtained curves could be a useful tool to define the thickness that the circular or pointed arch should have to withstand an earthquake of assigned intensity.

The experimental results on scaled arch models are not in perfect agreement with the expected theoretical ones, confirming the observations already present in the literature. In order to justify these results a probabilistic sensitivity analysis has been carried out by varying the geometrical parameters of the analysed arches, in the hypothesis of absence of correlation between them. Despite the adopted simplifications, the results appear to justify the discrepancies observed and lead to insight this aspect considering more consistent probabilistic models for the geometrical parameters, characterized by correlations that are in better agreement with the applications.

References

[1] R. Hooke, A description of helioscopes, and some other instruments, T.R. for John Martin Printer to the Royal Society, London, 1676.

[2] D. Gregory, Catenaria, Phil. Trans. Royal Society 19 (1695-1697) 637–652.

[3] J. Bernoulli, Varia posthuma. articul. xxix., Opera 2 (1744) 1119–1123.

[4] J. Stirling, Linee Tertii Ordinis Neutoniane, Impensis Edvardi Whistler, Bibliopolae Oxoniensis, 1717.

[5] G. Poleni, Memorie Istoriche della Gran Cupola del Tempio Vaticano, Padua: Nella Stamperia del Seminario, 1748.

[6] N. Cavalagli, V. Gusella, Dome of the basilica of santa maria degli angeli in Assisi: Static and dynamic assessment, International Journal of Architectural Heritage 9 (2) (2015) 157–175.

[7] N. Cavalagli, G. Gusella, Structural Investigation of 18th-Century Ogival Masonry Domes: From Carlo Fontana to Bernardo Vittone, Internationl Journal of Architectural Heritage 9 (3) (2015) 265–276.

[8] P. Couplet, De la pousse des voutes, Mémoires d l'Académie Royale des Sciences (1730) 117–141.

[9] M. Milankovitch, Theorie der druckkuerven, Zeitschrift fr Mathematik und Physik 55 (1907) 1–27.

[10] F. Foce, Milankovitch's theorie der druckkurven: Good mechanics for masonry architecture, Nexus Network Journal 9 (2) (2007) 185–210.

[11] H. Alexakis, N. Makris, Limit equilibrium analysis of masonry arches, Archive Applied Mechanics 84 (5) (2014) 757–772.

[12] N. Makris, H. Alexakis, The effect of stereotomy on the shape of the thrust-line and the minimum thickness of semicircular masonry arches, Archive of Applied Mechanics 83 (2013) 1511–1533.

[13] J. Heyman, The masonry arch, Ellis Horwood Ltd., Chinchester, 1982.

[14] J. Heyman, The safety of masonry arches, International Journal of Mechanical Sciences 11 (1969) 363–385.

[15] G. Cocchetti, G. Colasante, E. Rizzo, On the analysis of minimum thickness in circular masonry arches, Applied Mechanics Review 64 (5) (2011) 051002.1–22.

[16] A. Romano, J. Ochsendorf, The mechanics of gothic masonry arches, International Journal of Architectural Heritage 4 (1) (2010) 59–82.

[17] H. Alexakis, N. Makris, Minimum thickness of elliptical masonry arches, Acta Mechanica 224 (12) (2013) 2977–2991.

[18] C. Franciosi, Limit behaviour of masonry arches in the presence of finite displacements, International Journal of Mechanical Sciences 28 (7) (1986) 463–471.

[19] I. Oppenheim, The masonry arch as a four-link mechanism under base motion, Earthquake Engineering and Structural Dynamics 21 (1992) 1005–1017.

[20] P. Clemente, Introduction to dynamics of stone arches, Earthquake Engineering and Structural Dynamics 27 (1998) 513–522.

[21] L. De Lorenzis, M. DeJong, J. Ochsendorf, Failure of masonry arches under impulse base motion, Earthquake Engineering and Structural Dynamics 36 (2007) 2119–2136.

[22] M. DeJong, L. De Lorenzis, S. Adams, J. Ochsendorf, Rocking stability of masonry arches in seismic regions, Earthquake Spectra 24 (4) (2008) 847–865.

[23] H. Alexakis, N. Makris, Limit equilibrium analysis and the minimum thickness of circular masonry arches to withstand lateral inertial loading, Archive Applied Mechanics 84 (2014) 757–772.

[24] R. Dimitri, F. Tornabene, A parametric investigation of the seismic capacity for masonry arches and portals of different shapes, Engineering Failure Analysis 52 (2015) 1–34.

[25] L. Caporale, R. Luciano, L. Rosati, Limit analysis of masonry arches with externally bonded FRP reinforcements, Computer Methods in Applied Mechanics and Engineering 196 (1-3) (2006) 247–260.

[26] D. Oliveira, I. Basilio, P. Luoreno, Experimental Behavior of FRP Strengthened Masonry Arches, Journal of Composites for Construction 14 (3) (2010) 312–322.

[27] A. Caporale, L. Feo, D. Hui, R. Luciano, Debonding of FRP in multi-span masonry arch structures via limit analysis, Composite Structures 108 (2014) 586–865.

[28] G. Milani, A. Tralli, Recent developments in F.E. analysis of FRP reinforced masonry vaults: Case studies in Italy, Key Engineering Materials 624 (2015) 389–396.

[29] L. Severini, Analisi limite di archi in muratura in grandi spostamenti, Master Thesis. University of Perugia, Italy, 2013.